Research Square

Preprints are preliminary reports that have not undergone peer review.
They should not be considered conclusive, used to inform clinical practice,
or referenced by the media as validated information.

Robustness of Off-Axis Electron Vortices in Nonuniform Magnetic Fields

Hui-Dong Huang
Sun Yat-sen University
Qi Meng
Sun Yat-sen University
Zhi-Bin Wang
Sun Yat-sen University
Liang Lu
Sun Yat-sen University
Jian Chen
Sun Yat-sen University
Li-Ping Zou
zoulp5@mail.sysu.edu.cn

Sun Yat-sen University

Article

Keywords:

Posted Date: November 11th, 2026

DOI: https://doi.org/10.21203/rs.3.rs-11406949/v1

License: This work is licensed under a Creative Commons Attribution 4.0 International License.
Read Full License

Additional Declarations: No competing interests reported.

Robustness of Off-Axis Electron Vortices in Nonuniform Magnetic Fields

Hui-Dong Huang [1†], Qi Meng [1†], Zhi-Bin Wang [1], Liang Lu [1], Jian Chen [1*], Li-Ping Zou [1*]

[1*]Sino-French Institute of Nuclear Engineering and Technology, Sun Yat-Sen University, Zhuhai, 519082, Guangdong, China.

*Corresponding author(s). E-mail(s): chenjian5@mail.sysu.edu.cn; zoulp5@mail.sysu.edu.cn;
Contributing authors: huanghd26@mail2.sysu.edu.cn; mengq8@mail2.sysu.edu.cn; wangzhb8@sysu.edu.cn; luliang3@mail.sysu.edu.cn;
†These authors contributed equally to this work.

Abstract

Rotational symmetry protects the topological charge of on-axis electron vortices but not of off-axis vortices. We identify an additional SU(1,1) dynamical invariant that guarantees conservation of their intrinsic orbital angular momentum within the near-axis approximation. First-principles simulations of an off-axis electron vortex traversing a Glaser lens confirm this prediction, establishing a robust transport mechanism in axisymmetric nonuniform magnetic fields.

Introduction

Electron vortices carrying quantized orbital angular momentum (OAM) provide a controllable internal degree of freedom for free electrons [1–4], with versatile applications ranging from electron microscopy [5], quantum information [6] and magnetic diagnostics [7] to high-energy physics [8]. To date, their dynamics have been explored predominantly under strictly on-axis propagation in axisymmetric magnetic fields, where rotational symmetry guarantees conservation of the canonical OAM [9–15].

In practice, however, electron vortices inevitably propagate with some transverse misalignment. In axisymmetric but nonuniform magnetic fields, such as those in Glaser

lenses [16], the centroid then no longer coincides with the symmetry axis (Fig. 1). Although axial symmetry still guarantees conservation of the total canonical OAM, the intrinsic OAM, defined relative to the instantaneous centroid [17, 18], is not guaranteed by rotational symmetry alone. Whether it survives off-axis propagation in such nonuniform fields remains an open question. Dynamical invariants have previously been identified for on-axis vortex modes in nonuniform magnetic fields [12], but those invariants constrain the transverse mode structure rather than the centroid motion; the intrinsic OAM of off-axis states was not addressed. More broadly, the conservation of extrinsic OAM lies outside the scope of Noether's theorem. It emerges from an algebraic structure of the near-axis Hamiltonian rather than from a continuous symmetry, which may explain why it has remained unnoticed.

In this article, we show that, within the paraxial approximation [3], the intrinsic OAM of an off-axis vortex is exactly conserved during propagation through axisymmetric nonuniform magnetic fields, despite the absence of centroid-frame symmetry protection. This conservation arises from two exact constraints acting in concert: the axial symmetry of the external field fixes the total canonical OAM, while a hidden SU(1,1) dynamical invariant, identified with the extrinsic OAM, prevents any transfer of angular momentum into the intrinsic part.

We confirm this prediction with first-principles numerical simulations of an off-axis electron vortex traversing a Glaser lens. The simulations solve the full three-dimensional Schrödinger equation without imposing the paraxial approximation, while retaining only the near-axis vector potential, the latter being far less restrictive than the paraxial condition. The results demonstrate that the wavepacket preserves both its vortex structure and intrinsic OAM over a wide range of propagation distances and transverse offsets, even under field gradients far steeper than typical experimental conditions. These findings establish a robust mechanism for vortex transport in realistic electron-optical systems, where field inhomogeneity and beam misalignment are unavoidable.

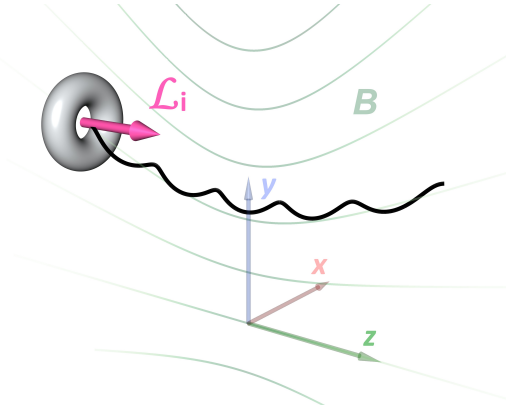


Fig. 1 An off-axis vortex wavepacket propagating through a magnetic lens. The centroid follows a helical trajectory that winds around the curved magnetic field lines, while the intrinsic OAM, defined relative to the centroid, is not protected by axial symmetry alone.

Results

Paraxial Theory

We consider an electron vortex in a magnetic field $\mathbf{B}$ rotationally symmetric about the z-axis. Let $-e$ ($e > 0$) be the electron charge. Near the axis, $\nabla \cdot \mathbf{B} = 0$ implies an axially varying longitudinal field $B(z)$ accompanied by a weak radial component at $\mathcal{O}(r_\perp)$, while off-axis corrections to B_z enter at $\mathcal{O}(r_\perp^2)$ [12, 14, 19]. To leading order, the vector potential in the symmetric gauge is

$$\mathbf{A} = \tfrac{1}{2} B(z)\, r_\perp \mathbf{e}_\theta. \tag{1}$$

The Hamiltonian is $\hat{H} = \hat{\boldsymbol{\pi}}^2/2m$ with $\hat{\boldsymbol{\pi}} = \hat{\mathbf{p}} + e\mathbf{A}$. The canonical OAM $\hat{\mathcal{L}} = (\hat{\mathbf{r}} \times \hat{\mathbf{p}})_z$ commutes with $\hat{H}$, so $\langle \hat{\mathcal{L}} \rangle$ is exactly conserved by axial symmetry. The intrinsic OAM, defined relative to the instantaneous centroid, decomposes as

$$\mathcal{L}_\mathrm{i} = \langle \hat{\mathcal{L}} \rangle - \mathcal{L}_\mathrm{ext}, \quad \mathcal{L}_\mathrm{ext} = \langle \hat{x} \rangle \langle \hat{p}_y \rangle - \langle \hat{y} \rangle \langle \hat{p}_x \rangle. \tag{2}$$

Hence $\mathcal{L}_\mathrm{i}$ evolves only through the extrinsic part $\mathcal{L}_\mathrm{ext}$, which is determined by the centroid's transverse motion. We note that $\mathcal{L}_\mathrm{ext}$ involves the canonical momentum, which is not gauge-invariant; as such it has no classical counterpart and its conservation cannot be inferred from classical theorems.

Under the paraxial approximation $\psi = e^{ikz}\chi$ with $|\partial_z^2 \chi| \ll k|\partial_z \chi|$ [3], the transverse dynamics obeys $i\hbar v\, \partial_z \chi = \hat{H}_\mathrm{eff} \chi$ ($v = \hbar k/m$). With $\omega_L(z) = eB(z)/2m$, the effective Hamiltonian is

$$\hat{H}_\mathrm{eff} = \frac{\hat{\mathbf{p}}_\perp^2}{2m} + \omega_L(z)\hat{\mathcal{L}} + \tfrac{1}{2} m \omega_L^2(z) \hat{r}_\perp^2. \tag{3}$$

We take the plane z_0 as the starting point of propagation, define $\hat{H}_0 \equiv \hat{H}_\mathrm{eff}(z_0)$, and work in the basis that diagonalizes $\hat{H}_0$. At this plane, the vector potential (1) yields a radial field $B_r = -\frac{1}{2} r_\perp B'(z_0)$ while its linear $r_\perp$-dependence ensures that $\hat{H}_0$ retains the algebraic form of a uniform-field Landau Hamiltonian. It is diagonalized by ladder operators $\hat{a} \equiv \hat{a}(z_0)$, $\hat{b} \equiv \hat{b}(z_0)$, with $[\hat{a}, \hat{a}^\dagger] = [\hat{b}, \hat{b}^\dagger] = 1$ and $[\hat{a}, \hat{b}] = [\hat{a}, \hat{b}^\dagger] = 0$. These are Schrödinger-picture operators, with all z-dependence carried by the state. Expectation values $\langle \cdot \rangle$ are understood to be taken with respect to $|\chi(z)\rangle$.

In terms of $\hat{a}$ and $\hat{b}$,

$$\hat{H}_0 = \hbar\omega_L(z_0)(2\hat{a}^\dagger \hat{a} + 1), \qquad \hat{\mathcal{L}} = \hbar(\hat{a}^\dagger \hat{a} - \hat{b}^\dagger \hat{b}). \tag{4}$$

The extrinsic OAM, defined in the Schrödinger picture, reads

$$\mathcal{L}_\mathrm{ext} = \hbar \left(|\langle \hat{a} \rangle|^2 - |\langle \hat{b}^\dagger \rangle|^2 \right). \tag{5}$$

The z-dependent part $\hat{V}(z) \equiv \hat{H}_{\rm eff}(z) - \hat{H}_0$ can be decomposed as

$$\hat{V}(z) = \Omega(z)\hat{\mathcal{L}} + \Lambda(z)\big(2\hat{K}_0 + \hat{K}_- + \hat{K}_+\big), \tag{6}$$

with $\Omega = \omega_L(z) - \omega_L(z_0)$ and $\Lambda = \hbar[\omega_L^2(z) - \omega_L^2(z_0)]/2\omega_L(z_0)$. Here

$$\hat{K}_0 = \tfrac{1}{2}(\hat{a}^\dagger\hat{a} + \hat{b}^\dagger\hat{b} + 1), \quad \hat{K}_+ = \hat{a}^\dagger\hat{b}^\dagger, \quad \hat{K}_- = \hat{a}\hat{b} \tag{7}$$

are the SU(1,1) generators, satisfying $[\hat{K}_0, \hat{K}_\pm] = \pm\hat{K}_\pm$ and $[\hat{K}_-, \hat{K}_+] = 2\hat{K}_0$ [20].

We now consider an off-axis vortex state at z_0 with $\mathcal{L}_{\rm i}(z_0) = \ell\hbar$, i.e. a state whose transverse centroid satisfies $\langle \mathbf{r}_\perp \rangle \neq 0$. According to the decomposition in Eq. (2), the extrinsic angular momentum $\mathcal{L}_{\rm ext}$ is determined by the centroid motion. For an on-axis state ($\langle \mathbf{r}_\perp \rangle = 0$), $\mathcal{L}_{\rm ext}$ vanishes identically; in uniform fields it may remain trivially constant [18], and its dynamical role has often been overlooked. In the off-axis, nonuniform regime, however, the non-zero centroid ($\langle \mathbf{r}_\perp \rangle \neq 0$) makes $\mathcal{L}_{\rm ext}$ a genuine dynamical variable whose conservation must be examined directly.

The term $\hat{H}_0 + \Omega(z)\hat{\mathcal{L}}$ can be removed by the unitary transformation

$$\hat{U}(z) = \exp\left[-\frac{i}{\hbar v}\int_{z_0}^{z} dz' \left(\hat{H}_0 + \Omega(z')\hat{\mathcal{L}}\right)\right]. \tag{8}$$

In the resulting interaction picture, $|\chi_I(z)\rangle = \hat{U}^\dagger(z)|\chi(z)\rangle$, the evolution is governed by the pure SU(1,1) Hamiltonian

$$\hat{H}_I(z) = \Lambda(z)\big(2\hat{K}_0 + e^{-i\Phi}\hat{K}_- + e^{i\Phi}\hat{K}_+\big), \tag{9}$$

with

$$\Phi(z) = \frac{2\omega_L(z_0)(z - z_0)}{v}. \tag{10}$$

To find a conserved quantity, we switch to the Heisenberg picture within the interaction frame. Defining $\hat{a}_I(z) = \hat{U}_I^\dagger(z)\hat{a}\,\hat{U}_I(z)$ and $\hat{b}_I^\dagger(z) = \hat{U}_I^\dagger(z)\hat{b}^\dagger\,\hat{U}_I(z)$, where $\hat{U}_I(z)$ is the formal evolution operator generated by $\hat{H}_I(z)$, i.e. $i\hbar v\,\partial_z\hat{U}_I = \hat{H}_I\hat{U}_I$ with $\hat{U}_I(z_0) = I$. A symmetric rotation

$$\hat{a}_R = e^{-i\Phi/2}\hat{a}_I, \qquad \hat{b}_R^\dagger = e^{i\Phi/2}\hat{b}_I^\dagger \tag{11}$$

then yields

$$i\hbar v\,\partial_z \begin{pmatrix} \hat{a}_R \\ \hat{b}_R^\dagger \end{pmatrix} = \mathcal{H}(z) \begin{pmatrix} \hat{a}_R \\ \hat{b}_R^\dagger \end{pmatrix}, \tag{12}$$

with

$$\mathcal{H}(z) = \begin{pmatrix} \Delta(z) & \Lambda(z) \\ -\Lambda(z) & -\Delta(z) \end{pmatrix}, \quad \Delta(z) = \hbar\omega_L(z_0) + \Lambda(z). \tag{13}$$

The expectation values $\langle \hat{a}_R \rangle_0$ and $\langle \hat{b}_R^\dagger \rangle_0$, taken with respect to the initial interaction-picture state $|\chi_I(z_0)\rangle$, obey the same equation (12). Defining $\mathbf{w} = (\langle \hat{a}_R \rangle_0, \langle \hat{b}_R^\dagger \rangle_0)^T$, one

has $i\hbar v\,\partial_z \mathbf{w} = \mathcal{H}\mathbf{w}$. Taking the conjugate transpose gives $-i\hbar v\,\partial_z \mathbf{w}^\dagger = \mathbf{w}^\dagger \mathcal{H}^\dagger$, from which

$$i\hbar v\,\partial_z(\mathbf{w}^\dagger \sigma_z \mathbf{w}) = \mathbf{w}^\dagger(\sigma_z \mathcal{H} - \mathcal{H}^\dagger \sigma_z)\mathbf{w}. \tag{14}$$

Since $\mathcal{H}^\dagger \sigma_z = \sigma_z \mathcal{H}$, the right-hand side vanishes, so the SU(1,1) norm $\mathbf{w}^\dagger \sigma_z \mathbf{w} = |\langle \hat{a}_R \rangle_0|^2 - |\langle \hat{b}_R^\dagger \rangle_0|^2$ is conserved.

To relate this conserved quantity to a physical observable, we return to the Schrödinger picture, where $\mathcal{L}_{\text{ext}}$ was expressed in terms of $\hat{a}$ and $\hat{b}^\dagger$ in Eq. (5). Tracing the sequence of transformations back to the original Schrödinger state, one finds that $\langle \hat{a}_R \rangle_0$ and $\langle \hat{b}_R^\dagger \rangle_0$ differ from $\langle \hat{a} \rangle$ and $\langle \hat{b}^\dagger \rangle$ by phases that drop out in the norm. Hence

$$\mathbf{w}^\dagger \sigma_z \mathbf{w} = |\langle \hat{a} \rangle|^2 - |\langle \hat{b}^\dagger \rangle|^2 = \mathcal{L}_{\text{ext}}/\hbar, \tag{15}$$

which is therefore constant.

Like the classical adiabatic invariant $\mu = m v_\perp^2/(2B)$ (the magnetic moment associated with the particle's gyromotion, approximately conserved when the field varies slowly compared with the cyclotron period [21]), $\mathcal{L}_{\text{ext}}$ is exactly conserved within the paraxial approximation, beyond which the conservation is only approximate (as seen in the numerical simulations below), and likewise constrains the transverse motion while leaving the detailed dynamics undetermined. Unlike μ, however, it is canonical and gauge-dependent, so it represents a purely quantum version of such an invariant. Although the near-axis Hamiltonian locally preserves the Landau eigenstructure at each z, an off-axis state feels transverse field components as it propagates, so its wavefunction can evolve in a complex way. The existence of this invariant protects the topological charge despite such complexity.

Numerical Simulation

To verify the robustness of the vortex structure and intrinsic OAM during off-axis propagation through a Glaser magnetic lens with on-axis profile $B(z) = B_0(1 + z^2/a^2)^{-1}$ [16, 22], we solve the full Schrödinger equation. We employ an operator-splitting Fourier pseudo-spectral method combined with a semi-Lagrangian integration scheme [23–25]. In our simulations, a vortex-electron wavepacket traverses a Glaser lens, as sketched in Fig. 1. The initial state is a Laguerre-Gaussian vortex wavepacket with a Gaussian longitudinal envelope [26], whose toroidal probability density $|\psi|^2$ is shown in Figs. 2(c) and 3(c).

We first examine the influence of magnetic non-uniformity, characterized by the length scale a, on the dynamics of an off-axis vortex electron, as shown in Fig. 2. The parameter is scanned over $a \in [40, 160]\, w_m$ while keeping the initial transverse offset fixed at $y_0 = 2\, w_m$. The resulting wavepacket snapshots at $t = 2.0\,|z_0|/v_0$ reveal a clear dependence on the magnetic-field variation scale. For a sufficiently smooth field profile [large a, Fig. 2(d)], the probability density exhibits transverse breathing while maintaining an almost ideal annular structure. As a decreases, the sharper longitudinal field gradient gives rise to increasingly pronounced non-paraxial effects, manifested by a noticeable spatial tilt of the wavepacket in the z–y plane [Fig. 2(e–f)]. Throughout the parameter scan, however, the vortex structure remains intact (see Supplemental Material for the full time evolution). The evolution of the intrinsic canonical orbital

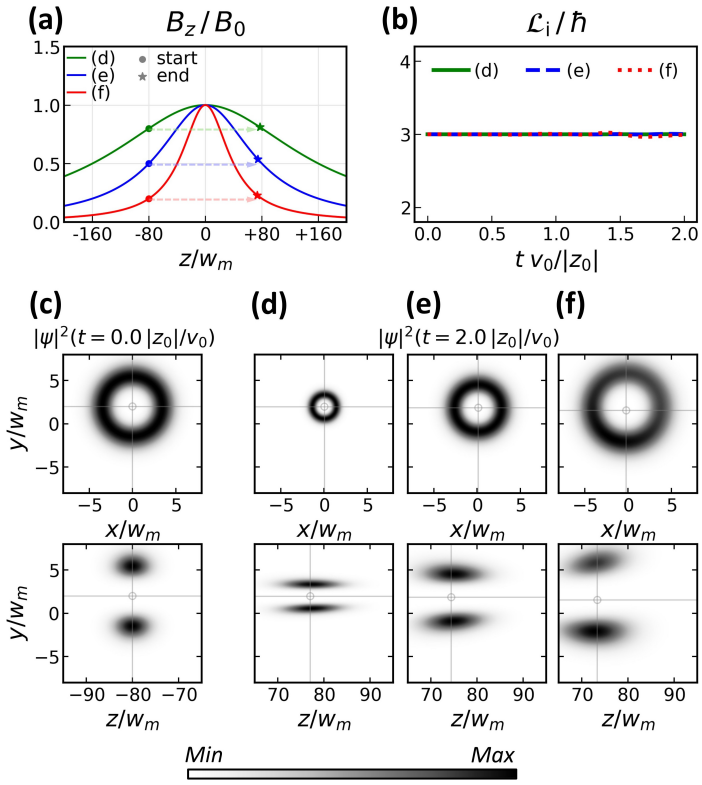


Fig. 2 Dynamics of an off-axis vortex-electron wavepacket in Glaser lenses with different characteristic lengths a. Panel (a) shows the longitudinal magnetic-field profiles $B_z(z)$ for $a = 160, 80, 40\,w_m$, and panel (b) the evolution of the intrinsic canonical OAM $\mathcal{L}_\mathrm{i}$. Panels (c–f) show the corresponding probability density $|\psi|^2$ at the initial time and at $t = 2.0|z_0|/v_0$. The initial wavepacket has topological charge $\ell = +3$, characteristic scales $w_\perp = 2\,w_m$ and $w_z = 4\,w_m$, centroid position $\mathbf{r}_0 = (0, +2, -80)\,w_m$, and axial speed $v_0 = (160\,w_m)/(6T_c)$. Here $B_0 = 0.02\,\mathrm{T}$, corresponding to $w_m = \sqrt{2\hbar/|eB_0|} = 0.256\,\mu\mathrm{m}$ and $T_c = 2\pi m/|eB_0| = 1.786\,\mathrm{ns}$.

angular momentum, $\mathcal{L}_\mathrm{i}$, is summarized in Fig. 2(b). Although stronger field gradients lead to larger dynamical modulations during propagation, the deviation from its initial value, $\Delta\mathcal{L}_\mathrm{i} = \mathcal{L}_\mathrm{i} - \ell\hbar$ with $\ell = +3$, remains below $0.04\,\hbar$ over the full parameter range. Even in the most nonuniform case [(f): $a = 40\,w_m$], the maximum relative deviation, $\varepsilon = \max|\Delta\mathcal{L}_\mathrm{i}/\ell\hbar|$, is only $\sim 1\%$.

We next investigate the influence of the initial transverse displacement y_0, as shown in Fig. 3. Here the lens profile is fixed at $a = 160\,w_m$, while the initial offset is varied over $y_0 \in [+2, +6]\,w_m$. The centroid trajectories $\bar{\mathbf{r}}$ in the z–y plane are shown in Fig. 3(a), exhibiting the characteristic undulating cyclotron motion superimposed on the overall guiding motion along the curved magnetic field lines (gray curves). Although larger offsets expose the electron to stronger transverse field components, the transverse probability density consistently preserves its circular symmetry and annular vortex profile for all cases considered [Figs. 3(d–f); see also Supplemental Material]. Likewise, the intrinsic OAM remains remarkably stable [Fig. 3(b)], with the maximum

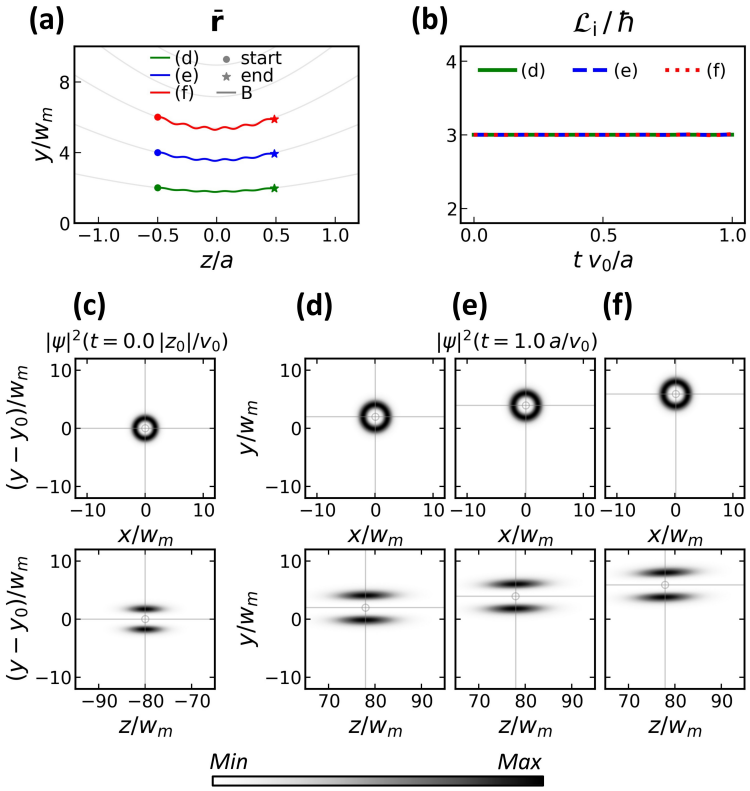


Fig. 3 Dynamics of an off-axis vortex-electron wavepacket for different initial transverse offsets y_0. Panel (a) displays the centroid trajectories $\bar{\mathbf{r}}$ in the z–y plane for $y_0 = +2, +4, +6\, w_m$, while panel (b) shows the evolution of the intrinsic canonical OAM $\mathcal{L}_\mathrm{i}$. Panels (c–f) show the corresponding probability density $|\psi|^2$ at the initial time and at $t = a/v_0$. The initial wavepacket has topological charge $\ell = +3$, characteristic scales $w_\perp = 1\, w_m$ and $w_z = 4\, w_m$, centroid position $\mathbf{r}_0 = (0, y_0, -0.5\, a)$, and axial speed $v_0 = a/(6T_c)$. The Glaser field is specified by $a = 160\, w_m$ and $B_0 = 0.02\,\mathrm{T}$, yielding the characteristic scales $w_m = 0.256\,\mu\mathrm{m}$ and $T_c = 1.786\,\mathrm{ns}$.

relative deviation reaching only $\varepsilon \simeq 0.3\%$ for the largest offset [(f): $y_0 = +6\, w_m$], corresponding to $|\Delta\mathcal{L}_\mathrm{i}| < 0.01\,\hbar$ throughout the evolution.

To verify that these small residual variations are not numerical artifacts, we performed grid-refinement tests for the results shown in Figs. 2(b) and 3(b). The percent-level residuals remain essentially unchanged under both coarser and finer spatial meshes (see Supplemental Material), indicating that the observed fluctuations in $\mathcal{L}_\mathrm{i}$ originate from the underlying quantum dynamics rather than numerical discretization errors.

We further examine the dependence on the initial intrinsic OAM by fixing the lens profile at $a = 160\, w_m$ and the initial offset at $y_0 = +2\, w_m$, while changing the topological charge over $\ell \in [-5, +5]$. The maximum relative deviation remains below $\varepsilon \lesssim 0.1\%$ for all values of ℓ, with no clear scaling relationship with respect to ℓ (see Supplemental Material).

Taken together, these simulations confirm that neither magnetic-field non-uniformity nor off-axis beam injection significantly affects the intrinsic OAM. Both the vortex structure and the intrinsic canonical OAM remain remarkably robust during electron transport through the magnetic lens.

Discussion

From a topological perspective, the vortex is characterized by the phase winding number around a closed contour C enclosing the phase singularity at the beam centroid [27], $\frac{1}{2\pi}\oint_C \boldsymbol{\nabla}_\perp \arg\phi \cdot d\boldsymbol{l} = \ell$. For the quadratic axisymmetric Hamiltonian (3), the wave function remains in the same azimuthal sector during propagation due to the hidden SU(1,1) dynamics, so the contour can be continuously transported without crossing a zero of the wave function. Consequently, the winding number cannot change, and the integer ℓ is a genuine conserved quantum number. In this model, the topological charge and the centroid-relative intrinsic OAM are represented by the same integer ℓ, so intrinsic-OAM conservation is accompanied by exact preservation of the vortex topology.

The small residual evolution of $\mathcal{L}_\mathrm{i}$ observed in our simulations follows from the full three-dimensional quantum dynamics. From the Heisenberg equations for $\hat{\mathbf{r}}$ and $\hat{\mathbf{p}}$, one obtains

$$\begin{aligned}\frac{\mathrm{d}\mathcal{L}_\mathrm{ext}}{\mathrm{d}t} = {}& m\big[\langle\hat{y}\rangle\,\mathrm{Cov}(\hat{\omega}_L^2,\hat{x}) - \langle\hat{x}\rangle\,\mathrm{Cov}(\hat{\omega}_L^2,\hat{y})\big] \\ &+ \big[\langle\hat{x}\rangle\,\mathrm{Cov}(\hat{\omega}_L,\hat{p}_x) - \langle\hat{p}_x\rangle\,\mathrm{Cov}(\hat{\omega}_L,\hat{x})\big] \\ &+ \big[\langle\hat{y}\rangle\,\mathrm{Cov}(\hat{\omega}_L,\hat{p}_y) - \langle\hat{p}_y\rangle\,\mathrm{Cov}(\hat{\omega}_L,\hat{y})\big],\end{aligned} \tag{16}$$

where $\hat{\omega}_L = \omega_L(\hat{z})$ and $\mathrm{Cov}(\hat{o}_1,\hat{o}_2) \equiv \langle\hat{o}_1\hat{o}_2\rangle - \langle\hat{o}_1\rangle\langle\hat{o}_2\rangle$. As $\langle\hat{\mathcal{L}}\rangle$ is conserved by axial symmetry, the residual evolution of $\mathcal{L}_\mathrm{i}$ seen in our simulations must originate from the right-hand side of Eq. (16).

To see when these covariance terms become appreciable, expand $\omega_L(\hat{z}) \simeq \omega_L(z_c) + \omega_L'(z_c)(\hat{z}-z_c)$ around the centroid $z_c \equiv \langle\hat{z}\rangle$. To leading order, $\mathrm{Cov}(\hat{\omega}_L,\hat{o}) \simeq \omega_L'\,\mathrm{Cov}(\hat{z},\hat{o})$, $\mathrm{Cov}(\hat{\omega}_L^2,\hat{o}) \simeq 2\omega_L\omega_L'\,\mathrm{Cov}(\hat{z},\hat{o})$ for $\hat{o} = \hat{x},\hat{y},\hat{p}_x,\hat{p}_y$. For a wavepacket of longitudinal extent w_z and transverse extent $w_\perp$, $\mathrm{Cov}(\hat{z},\hat{r}_\perp) \sim w_z w_\perp$ and $\mathrm{Cov}(\hat{z},\hat{p}_\perp) \sim w_z\,\hbar/w_\perp$, as these covariances measure the characteristic longitudinal–transverse correlations within the wavepacket.

Inserting these estimates into Eq. (16), each of the six terms scales as $|\omega_L'|w_z\hbar$ (the ω_L^2 terms carry an extra factor $m\omega_L w_\perp^2/\hbar \sim (w_\perp/w_m)^2$, which is $O(1)$ since $w_\perp \sim w_m$ in our simulations). With $\mathcal{L}_\mathrm{ext} \sim \hbar$ and dividing by the natural frequency scale ω_L yields the dimensionless control parameter

$$\frac{|d\mathcal{L}_\mathrm{ext}/dt|/\mathcal{L}_\mathrm{ext}}{\omega_L} \sim \frac{|\omega_L'|w_z}{\omega_L} \sim \frac{B'w_z}{B}, \tag{17}$$

which measures the fractional field variation across the wavepacket. When $B'w_z/B \ll 1$, the field is nearly uniform and the covariance terms are frozen out; when it approaches unity, the wavepacket resolves the inhomogeneity and $\mathcal{L}_\mathrm{ext}$ can evolve

appreciably. For the Glaser field $B(z) = B_0(1 + z^2/a^2)^{-1}$, $B'/B \sim 1/a$, so the ratio reduces to w_z/a.

In our simulations this ratio reaches $w_z/a \lesssim 10^{-1}$ (the field changes by $\sim 10\%$ over the wavepacket), a regime far more extreme than typical electron-optical conditions, chosen deliberately to expose any beyond-paraxial corrections. Even under this strict test, $\mathcal{L}_\mathrm{i}$ deviates by only a few percent. In practical settings, where $w_z \ll B/B'$, the field is effectively uniform across the wavepacket, the covariances are negligible, and $\mathcal{L}_\mathrm{i}$ is conserved. Importantly, the theoretical results rely only on the near-axis vector potential of Eq. (1), not on the specific Glaser profile used in the numerical simulation. The mechanism thus applies generally to axisymmetric magnetic systems described by the same near-axis model, including magnetic mirrors and solenoids [14, 19, 26].

Beyond electron optics, the demonstrated robustness also supports emerging proposals for off-axis vortex-particle scattering employing transverse beam-center offsets as tunable impact parameters [28], by preserving the intrinsic OAM during transport through axisymmetric nonuniform magnetic fields.

Conclusion

We have shown that off-axis vortex electrons possess a previously unrecognized robustness in nonuniform axisymmetric magnetic fields. Although rotational symmetry alone does not protect the intrinsic OAM defined with respect to the instantaneous centroid, its conservation follows from the combined action of this geometric symmetry and a hidden dynamical invariant associated with the SU(1,1) algebra within the near-axis approximation. Numerical simulations of vortex-electron propagation through Glaser magnetic lenses verify this prediction and demonstrate stable transport of the vortex structure under magnetic-field inhomogeneity and beam misalignment. The mechanism is expected to extend to a broad class of axisymmetric electron-optical systems.

Supplementary information. See Supplemental Material at [URL to be inserted by publisher] for derivations of the Landau-level algebra, the SU(1,1) structure, and the time evolution of the extrinsic canonical OAM, along with the numerical method, additional simulations, and movies of the wavepacket evolution.

Acknowledgements. We thank Pengming Zhang for valuable comments.

Declarations

Funding. The work was supported by the National Key R&D Program of China (No. 2024YFE0109802), the National Natural Science Foundation of China (Grant No. 12175320), and the Guangdong Basic and Applied Basic Research Foundation (Grant No.2026A1515010999).

Conflict of Competing interests. The authors declare that they have no competing interests.

Ethics approval and consent to participate. Not applicable.

Consent for publication. Not applicable.

Data availability. The numerical data and scripts for reproducing the figures are publicly available in Zenodo at https://doi.org/10.5281/zenodo.21668676.

Materials availability. Not applicable.

Code availability. The custom computer code used to generate the findings of this study is openly available in the Github repository at https://github.com/Leonardo-HHD/GlaserVortex and has been permanently archived in Zenodo at https://doi.org/10.5281/zenodo.21668677 under an GNU v3.0 license.

Author contribution. All authors contributed substantially to this work. Hui-Dong Huang and Qi Meng contributed equally. Hui-Dong Huang developed the numerical code, performed the simulations, analyzed the data, and drafted the manuscript. Qi Meng developed the theoretical framework, interpreted the results, and drafted the manuscript. Zhi-Bin Wang and Liang Lu contributed to refining the results and their presentation. Jian Chen and Li-Ping Zou conceived and supervised the project, proposed the research idea, verified the results, reviewed and revised the manuscript, and acquired funding.

References

[1] Bliokh, K.Y., Bliokh, Y.P., Savel'ev, S., Nori, F.: Semiclassical dynamics of electron wave packet states with phase vortices. Physical Review Letters **99**(19), 190404 (2007) https://doi.org/10.1103/PhysRevLett.99.190404

[2] Verbeeck, J., Tian, H., Schattschneider, P.: Production and application of electron vortex beams. Nature **467**(7313), 301–304 (2010) https://doi.org/10.1038/nature09366

[3] Bliokh, K.Y., Ivanov, I.P., Guzzinati, G., Clark, L., Van Boxem, R., Béché, A., Juchtmans, R., Alonso, M.A., Schattschneider, P., Nori, F., Verbeeck, J.: Theory and applications of free-electron vortex states. Physics Reports **690**, 1–70 (2017) https://doi.org/10.1016/j.physrep.2017.05.006

[4] Lloyd, S.M., Babiker, M., Thirunavukkarasu, G., Yuan, J.: Electron vortices: Beams with orbital angular momentum. Reviews of Modern Physics **89**(3), 035004 (2017) https://doi.org/10.1103/RevModPhys.89.035004

[5] Juchtmans, R., Béché, A., Abakumov, A., Batuk, M., Verbeeck, J.: Using electron vortex beams to determine chirality of crystals in transmission electron microscopy. Physical Review B **91**(9), 094112 (2015) https://doi.org/10.1103/PhysRevB.91.094112

[6] Löffler, S., Schachinger, T., Hartel, P., Lu, P.-H., Dunin-Borkowski, R.E., Obermair, M., Dries, M., Gerthsen, D., Schattschneider, P.: A quantum logic gate for free electrons. Quantum **7**, 1050 (2023) https://doi.org/10.22331/q-2023-07-11-1050

[7] Barrows, F., Petford-Long, A.K., Phatak, C.: 3D magnetic imaging using electron vortex beam microscopy. Communications Physics **5**(1), 1–11 (2022) https://doi.org/10.1038/s42005-022-01082-z

[8] Ivanov, I.P.: Promises and challenges of high-energy vortex states collisions. Progress in Particle and Nuclear Physics **127**, 103987 (2022) https://doi.org/10.1016/j.ppnp.2022.103987

[9] Bliokh, K.Y., Schattschneider, P., Verbeeck, J., Nori, F.: Electron vortex beams in a magnetic field: A new twist on landau levels and aharonov-bohm states. Physical Review X **2**(4), 041011 (2012) https://doi.org/10.1103/PhysRevX.2.041011

[10] Greenshields, C.R., Stamps, R.L., Franke-Arnold, S., Barnett, S.M.: Is the Angular Momentum of an Electron Conserved in a Uniform Magnetic Field? Physical Review Letters **113**(24), 240404 (2014) https://doi.org/10.1103/PhysRevLett.113.240404

[11] Zou, L., Zhang, P., Silenko, A.J.: General quantum-mechanical solution for twisted electrons in a uniform magnetic field. Physical Review A **103**(1), 010201 (2021) https://doi.org/10.1103/PhysRevA.103.L010201

[12] Melkani, A., van Enk, S.J.: Electron vortex beams in nonuniform magnetic fields. Physical Review Research **3**(3), 033060 (2021) https://doi.org/10.1103/PhysRevResearch.3.033060

[13] Karlovets, D., Grosman, D., Pavlov, I.: Angular momentum dynamics of vortex particles in accelerators. Physical Review Letters **136**(8), 085002 (2026) https://doi.org/10.1103/gsrz-cscl

[14] Filina, N.V., Baturin, S.S.: Universal analytic solution for the quantum transport of structured matter waves in magnetic optics. Physical Review A **113**(2), 021302 (2026) https://doi.org/10.1103/y1d1-dzqh

[15] Filina, N.V., Baturin, S.S.: Effective Caldirola-Kanai model for accelerating twisted Dirac states in nonuniform axial fields. Physical Review A **113**(5), 053315 (2026) https://doi.org/10.1103/lxww-h7r2

[16] Szilagyi, M.: Electron and Ion Optics. Microdevices. Springer, New York, US (2012). https://doi.org/10.1007/978-1-4613-0923-9

[17] O'Neil, A.T., MacVicar, I., Allen, L., Padgett, M.J.: Intrinsic and extrinsic nature of the orbital angular momentum of a light beam. Physical Review Letters **88**(5), 053601 (2002) https://doi.org/10.1103/PhysRevLett.88.053601

[18] Greenshields, C.R., Franke-Arnold, S., Stamps, R.L.: Parallel axis theorem for free-space electron wavefunctions. New Journal of Physics **17**(9), 093015 (2015) https://doi.org/10.1088/1367-2630/17/9/093015

[19] Zou, L., Zhang, P., Silenko, A.J.: Production of twisted particles in magnetic fields. Journal of Physics B: Atomic, Molecular and Optical Physics **57**(4), 045401 (2024) https://doi.org/10.1088/1361-6455/ad23f7

[20] Gerry, C.C.: Correlated two-mode SU(1, 1) coherent states: Nonclassical properties. Journal of the Optical Society of America B **8**(3), 685 (1991) https://doi.org/10.1364/JOSAB.8.000685

[21] Northrop, T.G.: The Adiabatic Motion of Charged Particles. Interscience, New York, US (1963)

[22] Khan, S.A., Jagannathan, R.: Quantum mechanics of round magnetic electron lenses with glaser and power law models of b(z). Optik **229**, 166303 (2021) https://doi.org/10.1016/j.ijleo.2021.166303

[23] Jin, S., Zhou, Z.-N.: A semi-lagrangian time splitting method for the schrödinger equation with vector potentials. Communications in Information and Systems **13**(3), 247–289 (2013) https://doi.org/10.4310/CIS.2013.v13.n3.a1

[24] Caliari, M., Ostermann, A., Piazzola, C.: A splitting approach for the magnetic schrödinger equation. Journal of Computational and Applied Mathematics **316**, 74–85 (2017) https://doi.org/10.1016/j.cam.2016.08.041

[25] Gutleb, T.S., Mauser, N.J., Ruggeri, M., Stimming, H.P.: A time splitting method for the three-dimensional linear pauli equation. Computational Methods in Applied Mathematics **24**(2), 407–420 (2024) https://doi.org/10.1515/cmam-2023-0094

[26] Sizykh, G.K., Chaikovskaia, A.D., Grosman, D.V., Pavlov, I.I., Karlovets, D.V.: Nonstationary laguerre–gaussian states in a magnetic field. Progress of Theoretical and Experimental Physics **2024**(5), 053–02 (2024) https://doi.org/10.1093/ptep/ptae052

[27] Lubk, A., Clark, L., Guzzinati, G., Verbeeck, J.: Topological analysis of paraxially scattered electron vortex beams. Physical Review A **87**(3), 033834 (2013) https://doi.org/10.1103/PhysRevA.87.033834

[28] Yang, Y., Ivanov, I.P.: Universal features of high-energy scattering of laguerre-gaussian states. Physical Review D **113**(11), 116020 (2026) https://doi.org/10.1103/h5bv-6sl5

Supplementary Files

This is a list of supplementary files associated with this preprint. Click to download.

- SM.pdf
- MovieS1.y02a160wr2.mp4
- MovieS4.y02a160wr1.mp4
- MovieS3.y02a40wr2.mp4
- MovieS5.y04a160wr1.mp4
- MovieS2.y02a80wr2.mp4
- MovieS6.y06a160wr1.mp4